The Upgraded Kharkiv V. N. Karazin National University Radiophysical Observatory

L.F.Chernogor, K.P.Garmash, V.A.Podnos, V.T.Rozumenko, A.M.Tsymbal, O.F.Tyrnov

Kharkiv V. N. Karazin National University, 4 Svoboda Square, Kharkiv, 61077 Ukraine

E mail Leonid.F.Chernogor@univer.kharkov.ua

Accepted: December 1, 2011

Abstract. The Kharkiv V. N. Karazin National University Radiophysical Observatory clustered instruments are located at two sites, Gaidary (49°37'51" N; 36°19'40.1" E) and Grakovo (49°38'49" N; 36°56'07" E), where sample clock synchronization is accomplished by using GPS receivers. It is a powerful tool for identifying hidden linkages between different altitudes from the D region to GPS orbits. The findings from some experimental studies are illustrated. The MF–HF radar (Gaidary) simultaneously employs the differential absorption, spaced antenna, and the ionosonde techniques. HF Doppler sounding system comprises an HF Doppler radar at vertical incidence at Gaidary (it simultaneously makes soundings at three frequencies) and a passive radar system at Grakovo (it simultaneously observes four frequencies in the 30 kHz – 3 MHz band and eight frequencies in the 1 – 31 MHz band with a velocity resolution of a few m s^{-1} in most cases). Low-Earth orbit Cicada/Cicada-M and GPS/GLONASS navigation satellite TEC observations are made at Gaidary and Kharkiv City. Since 2001, the fluxgate magnetometer (Grakovo) has acquired measurements in the south-north (H component) and west-east (D) directions at half-second intervals in the 0.001 – 1 Hz frequency band within which the internal noise varies from 0.5 pT at f = 1 Hz to 50 pT at f = 0.01Hz. The three-axis saturable-core magnetometer (Gaidary) acquires measurements in the two frequency bands, 0.01 – 0.1 Hz and 0.1 – 5 Hz, where the internal noise level does not exceed 0.075 nT.

Keywords: magnetometer, Glonass receiver, radar, software, spectral estimation

Introduction

The Kharkiv V. N. Karazin National University Radiophysical Observatory clustered instrument capabilities have continuously been upgraded (Tyrnov et al., 1994; Garmash et al., 1999a; Garmash et al., 1999b; Garmash et al., 2003), and this paper mainly focuses on the upgrades to the instrumentation located at the Grakovo site (49°38'49" N; 36°56'07" E) where the industrial noise level is the lowest in the region. The upgraded instruments include a fluxgate magnetometer, a passive radar system (four frequencies in the 30 kHz – 3 MHz band and eight frequencies in the 1 – 31 MHz band) at the Grakovo site. Illustrations of findings from satellite radio beacon receivers, which receive signals from low-Earth orbit Cicada/Cicada-M and GPS/GLONASS satellites at Gaidary and Kharkiv City, and a radar for simultaneously measuring the electron density profile from the D region to the F-layer peak altitude at the Gaidary site (49°37'51" N; 36°19'40.1" E) are also presented.

Magnetometer

The magnetometer and data recording system developed and produced in the Department of Space Radio Physics have acquired measurements in the south-north (H component) and west-east (D) directions since 2001. The magnetometer design is based on the IM-II fluxgate magnetometer produced by the Institute of the Earth Physics, Academy of Sciences, USSR in the late 1980s. It is capable of taking measurements over a period range of 1 – 1000 s, and it has the measurement precision of 0.5 – 50 pT in the 1 – 100 s period range, respectively. The calibration means permits the test of all measurement circuitry, including the sensors. Figure 1 shows the block diagram illustrating the basic layout of the magnetometer. The IM-II magnetometer is connected to the dedicated microcontroller-recorder (MCR). The recorder design is based on the Atmel AVR ATmega128 microcontroller and the non-volatile Dallas Semiconductor DS12887 clock. The microcontroller code digitizes and preliminarily filters magnetometer signals over 0.5 s time intervals, as well as stores the filtered samples and their timing in the non-volatile USB flash drive. In addition, the MCR serves as an uninterrupted power supply by controlling the standard outlet voltage and by charging 12 V 60 A-h rechargeable battery. In case of the electrical grid failure, the magnetometer is switched over to the rechargeable battery, and in case of a battery complete discharge, the battery is disconnected. The four button input keyboard is used to program the controller, and the controller state is displayed on the LCD panel. The MCR selects date and time from the GPS data in NMEA format obtained by the BR-304 receiver, sends them further to the instrumentation for passively monitoring the ionosphere, and daily adjusts its own non-volatile clock. The time synchronization precision is not worse than ±0.1 s over a 24-h time interval. The upgraded magnetometer consumes 6 watts of power, which suffices for self-sufficient operation during 120 h. Figure 2 shows a photograph of the magnetometer.

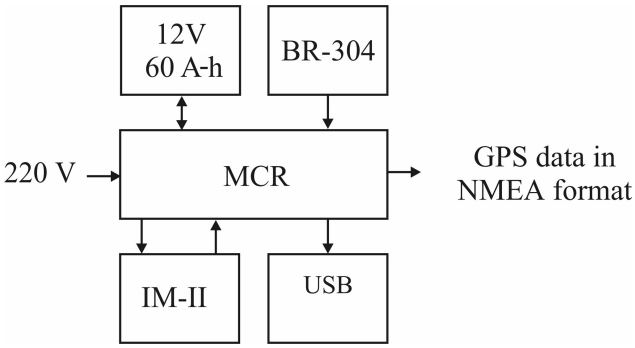

Figure 1. Fluxgate magnetometer block diagram. BR-304 is GPS receiver; 12 V 60 A-h denotes power supply (storage battery); MCR is microcontroller-recorder; IM-II is induction fluxgate magnetometer; USB is 4 gigabyte non-volatile USB flash drive.

Figure 2. A photograph of the upgraded magnetometer.

The magnetometer data have been validated and their quality has been verified using the data from the LEMI-017 Meteomagnetic Station produced by the Lviv Center of the Institute of Space Research and located nearby at the Low Frequency Observatory of the Institute for Radio Astronomy of the Ukrainian National Academy of Sciences near Martovoe Village (49°56'0.5" N; 36°57'10" E), Pechenezhskiy Region, Kharkiv Province. The distance between the instruments is equal to about 35 km in the north-south direction. The comparison was based on geomagnetic field samples acquired with a 1-s sampling interval and a precision of 10 pT on August 10, 2008.

The cross-correlation between the H and D components of the geomagnetic field in the 10 – 100 s period range was estimated over 1-h time intervals. The Fourier transform was used to filter the samples in trapezoidal 4096-sample windows with the upper trapezoid base length of 1 h, the 10 – 100 s period harmonics were subsequently selected, and the inverse Fourier transform was performed. The central 3600 of 4096 filtered harmonics were used in further analysis.

Since the frequency and phase responses of the IM-II fluxgate magnetometer correspond to those of a differencing circuit with a time constant of 3 s, the nonlinear frequency response was mitigated by additionally transforming the cosine and sine spectral signal components as follows:

$$U_{c,in} + iU_{s,in} = \frac{K_c U_{c,out} + K_s U_{s,out}}{K_c^2 + K_s^2} + i\frac{K_c U_{s,out} - K_s U_{c,out}}{K_c^2 + K_s^2},$$

where

$$K_c = \frac{1}{1+(\omega\tau)^{-2}}, \qquad K_s = \frac{K_c}{\omega\tau},$$

$U_{in}(\omega) = U_{c,in}(\omega)\cos(\omega t) + iU_{s,in}(\omega)\sin(\omega t)$ and
$U_{out}(\omega) = U_{c,out}(\omega)\cos(\omega t) + iU_{s,out}(\omega)\sin(\omega t)$

are the complex input and output signal harmonics, respectively, $\omega = 2\pi f$ is a radian frequency, i is the imaginary unit. The LEMI-017 magnetometer frequency response is flat and its data do not require additional transformations.

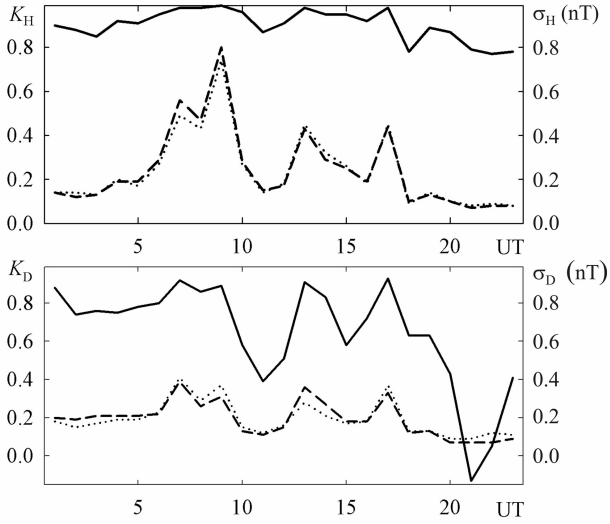

Figure 3. Cross-correlation coefficients *K* (solid lines) versus time estimated over 1 h intervals for a cross-correlation between 10 – 100 s period variations in the H (top panel) and D (lower panel) geomagnetic field components that were registered at the spaced observation sites Grakovo and Martovoe on August 10, 2008. The root-mean-square errors for the Grakovo site are designated by dotted lines and by dashed curves for the Martovoe site.

Figure 3 shows the results of the calculations. The correlation coefficient is high (especially in the H component), attains a value of 0.99, and the r.m.s. values of the variations are almost equal in both magnetometers. The offset between the maximum locations in the correlation functions does not exceed a magnetometer time resolution of ±1.5 s. This indicates that the observed processes are mainly synchronous and obviously of magnetospheric origin. The correlation between the D components sometimes decreases to 0.4–0.5 or even complete decorrelation occurs when $|K_D| < 0.2$. At these points of time, the r.m.s. values decrease to 0.1 nT and

smaller. Such a behavior can be explained either by an increase in local interference or by a manifestation of smaller variations of ionospheric origin, which are not synchronous at the spaced observation sites. Also, the D component variations of magnetospheric origin are generally smaller than the H component variations.

Instrumentation and software for monitoring the ionosphere

The instrumentation is used for studying variations in radio waves reflected from the ionosphere. It can operate as a passive HF Doppler radar at oblique incidence or as a panoramic monitor of radio interference. The Doppler radar intercepts signals from broadcasting, radionavigation, time and frequency service, and other transmitters.

The panoramic studies are based on the statistical analysis of the electromagnetic field, which is a superposition of narrow-band emissions of remote radio transmitters and noise-like radio interference generated by natural and anthropogenic sources. The frequency band is chosen to be wide to intercept a large enough number of narrow-band sources of emission.

The software for the passive radar and the panoramic monitor includes computer codes for data acquisition and processing, and for testing and controlling the equipment.

The instrumentation includes the following: (1) an antenna signal splitter, (2) a PC, (3) a unit for microcomputer-controlling the synthesizer-type R-399A and R-391V2 radio receivers in the 1 – 32 MHz and 50 kHz – 2 MHz bands, respectively; these receivers also perform the first two frequency conversions and their main amplification, (4) the C6-31 frequency synthesizer used as the third heterodyne, and (5) units for performing the third frequency conversion and low-pass filtering.

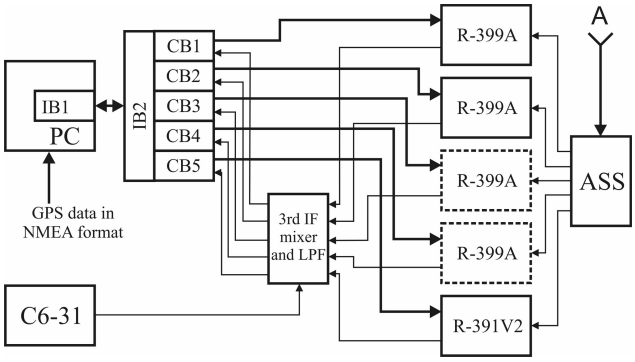

Figure 4. Functional block diagram of the instrumentation for passively monitoring the ionosphere. PC is personal computer, IB1 and IB2 are buffer interfaces, CB1 – CB5 are receiver control circuit boards, R-399A is decameter wave receiver (dotted-lined receiver outlines designate the possibility of their connection in the future), R-391V2 is hectometer wave receiver, A is receiving antenna, ASS is antenna signal splitter, C6-31 is frequency synthesizer for 3rd oscillator.

The 5 MHz local oscillator signal in one of the receivers is shared by all other receivers and is used for the 1 MHz encode clock in the analog-to-digital converter (ADC). The temperature-controlled radio receiver and C6-31 frequency synthesizer oscillators ensure long-term frequency instability of no less than $5 \cdot 10^{-8}$. As will be shown below, the instability is almost an order of magnitude less.

Doppler measurements are the main mode of operation, for which the facility functional block diagram is presented in Figure 4. The control unit receives binary code information via the IB1 and IB2 interface blocks and stores it in the control circuit board (CB1–CB5) internal registers. The information is comprised of the following: the setting for the radio receiver mode of operation, the frequency of received signal, the intermediate frequency amplifier (IFA) bandwidth, the IFA gain, and a front-end attenuator reduction level. The IFA gain is set by the 10-bit digital-to-analog converter (DAC), which is installed on the control circuit board.

The mode of operation of the radio receivers is programmable and this permits a single receiver to take measurements cyclically over several radio circuit paths and to set the gain for each frequency, which permits the spectral and time resolutions to be maintained high enough.

The signal at the radio receiver antenna input connections comes from the antenna signal splitter (ASS). The signals from the second 215 kHz IF amplifier outputs within the 300 Hz bandwidth are then fed into the third IF frequency mixers and low-pass filters (3rd IF & LPF). The analog signals in the 300 Hz band are fed into the F7077M/1 10-bit ADC placed at the respective control circuit boards where they are converted into digits at a sampling frequency of 600 samples per second. The digitized data are fed into the computer for further processing in real time, where they are low-pass filtered and decimated by a factor of 15.

The filtering is performed with an optimal band-pass Finite Impulse Response filter (Rabiner and Gold, 1975) which is designed by specifying the frequency range of the band, the passband, the attenuation of stopbands and the ripple of passbands. The maximum stopband attenuation optimality criterion is applied when all other parameters are specified.

The filter with 121 taps has a bandwidth of 0.04 times the sampling frequency, f_s, between the 10-dB cutoff frequencies, the passband center frequency of $0.25f_s$, and a stopband with 40 dB minimum attenuation. Figure 5 shows the filter frequency response $S(\omega) = 20\log_{10}[U_{out}(\omega) / U_{in}(\omega)]$. For f_s =600 Hz, the output signal central frequency is equal to 150 Hz, and the bandwidth to about 20 Hz.

The sequent decimation by a factor of 15 converts the signal into a signal in a frequency band from 0 to 20 Hz with a sampling frequency of 40 samples per second. These data in blocks of 512 samples (12.8-s measurement segment), together with a file header, are stored in a single diurnal data file. Each data block header contains the recording start time and

the frequency of the signal received. The blocks are registered each 15 s. The recording start time is determined with an error of ±0.1 s by means of the GPS receiver installed in the magnetometer and data recording system.

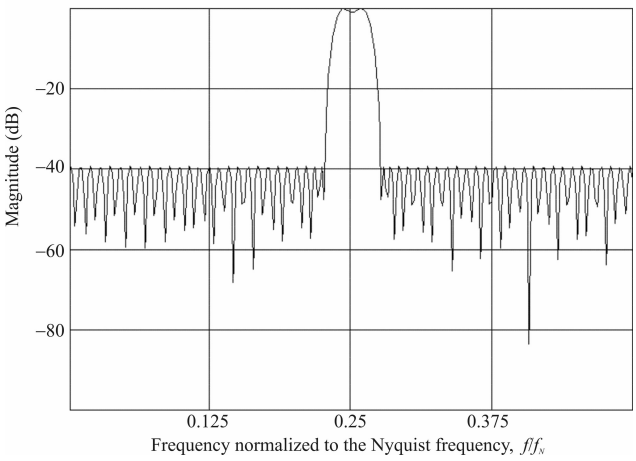

Figure 5. Filter frequency response

In order to avoid fading and receiving channel overloading, the measurement computer code also controls the level of the signal received, as well as performs the automatic control of the current values of the IF amplifier gain and of the receiver input attenuators. These current values are taken into account in evaluating the amplitude of the digital signals stored in the data file.

The algorithm for Doppler data processing retrieves from a diurnal data file the data for the signal with a desired frequency. Further, the algorithm estimates spectra with required accuracy and spectral resolution, identifies the main modes present in the radio signal (magnetoionic components or rays reflected from different ionospheric layers), and tracks the dynamics of these modes.

The spectral estimation based on the Fourier transform inherently has the drawbacks that the sample window influences the spectral resolution and a finite-length time sequence produces a fixed frequency sequence. Thus, the sequence of a 12.8 s length produces a spectral resolution of ~0.2 – 0.3 Hz for the signal-to-noise ratio of ~10 – 8 dB (Marple, 1987), which is of the order of Doppler frequency fluctuations observed in HF signals reflected from the ionosphere.

Another approach exploits autoregressive (AR) parameter estimation (Marple, 1987). When the signal-to-noise ratio is of the order of or exceeding 10 dB, the time series is well modeled as a finite number of strong modes. The AR parameters are calculated by jointly minimizing the minimum mean square errors of the direct and reverse linear predictors (the modified covariance technique (Marple, 1987)). The spectra calculated by employing these AR coefficients permit the frequency of the mode to be estimated with an error of 0.01 – 0.02 Hz and a spectral resolution of 0.05 – 0.06 Hz over a data set of 12.8 s.

The width of AR spectral lines is small, specifically, less than 0.03 Hz. Therefore, the spectrum dynamics is difficult to follow if the change in the frequency of a mode exceeds the width of a line over a time interval of 15 s. On the other hand, the block structure of the data prevents employing the moving average approach since the data series are acquired with gaps in time and phase. To calculate spectra over the gaps, we employ the inter-block linear interpolation of the AR coefficients. The dynamics of the spectral content can confidently be monitored for the gaps of up to 7.5 s. Therefore, the basic spectra are first calculated from the data in the blocks, and then the interpolated spectra are estimated. The duration of the gap is dependent on the number of channels, which one receiver digitizes, and therefore the number of interpolated spectra varies from one to seven.

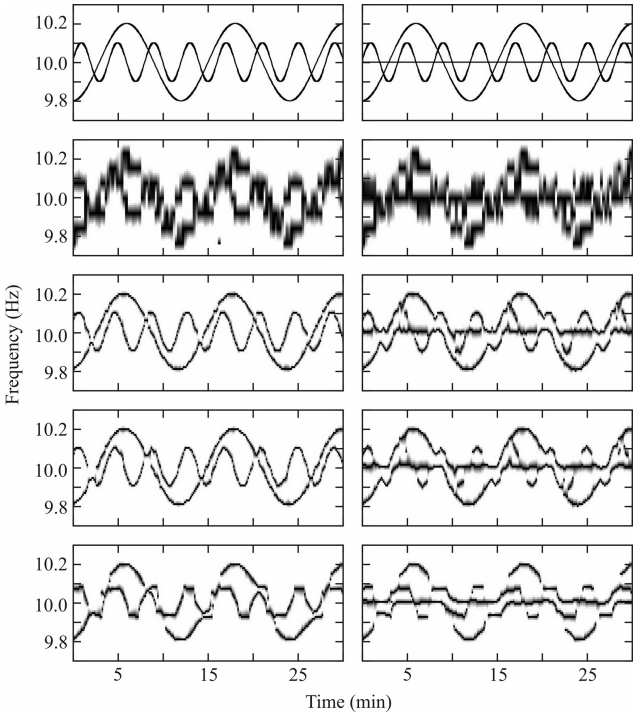

Figure 6 Quality of FFT and autoregressive (AR) spectral estimation vs. the magnitude of a gap between the data blocks. The plots from top to bottom represent (1) model signal dynamic spectra, (2) FFT dynamic spectra for 15-s gap between the data blocks of 512 samples (12.8-s measurement segment); (3), (4), (5) AR spectra for 15-s, 30-s, and 60-s gap between the data blocks, respectively. The signal-to-noise ratio is equal to 20 dB.

To study the dependence of the quality of this spectral estimation technique on the magnitude of a gap and on the signal-to-noise ratio, numerical simulations have been performed. A series of data blocks of 512 samples uniformly distributed over 12.8-s segment were generated. The data were modeled as a sum of two or three sinusoids of equal amplitudes and white Gaussian noise, while the signal-to-noise ratio varied from 10 dB to 40 dB. The total duration of

the time series was equal to 30 min and the time interval between the beginnings of the blocks was equal to 15 s. The first sinusoid varied its frequency sinusoidally from 9.9 Hz to 10.1 Hz with a period of 4 min, the second sinusoid varied its frequency anti-cosinusoidally from 9.8 Hz to 10.2 Hz with a period of 12 min, and the third sinusoid had a constant frequency of 10 Hz. In the top panels in Figure 6 are shown the plots of the model sinusoids' frequencies, consisting of two (on the left-hand side) and three (on the right-hand side) sinusoids.

Each data block in the time series was subjected to spectral analysis. The results were depicted as dynamic spectra, frequency vs. time dependencies, with amplitude on a grey scale, varying from black at the local maximum to white at the local minimum. Figure 6 shows the dynamic FFT spectra (the second panel from the top), the AR spectra (the third to fifth panels from the top for 15-s, 30-s, and 60-s gap between the data blocks with one, three, and seven interpolated spectra between each pair of the basic AR spectra, respectively).

The FFT spectra distinctly reveal discrete frequency grid with spacing of 0.08 Hz, and the spectral maxima are wide enough. As a result, the model consisting of two sinusoids is blurred, while in the three sinusoid model, the sinusoid with frequency variations of ±0.1 Hz is disguised by the sinusoid with constant frequency. The AR spectra are evidently much better. They permit easy reconstruction of two sinusoids, and some difficulties arise during the restoration of three sinusoids, which is associated with a large number of intersections between the sinusoids' traces. The finite spectral resolution, which is determined by the data block finite length, results in gaps and in false connections between the traces of different sinusoids. The three pairs of graphs at the bottom of Figure 6 illustrate the dependence of AR spectra on the gap between the data blocks.

In the fourth from the top row of graphs, each second basic spectrum was processed and three AR interpolated spectra between them were calculated. In the bottom row of graphs, each fourth basic spectrum was processed and seven AR interpolated spectra between them were calculated. The last two rows of graphs correspond to cyclically taking measurements by one receiver over two and four different radio circuits, respectively. It is evident that the difference between the third and fourth row from the top graphs are small, while a significant distortion can be seen in the shape of frequency deviations in the second model sinusoid. As a result, a further increase in the gap between the data blocks is obviously impossible and thus the number of radio circuits processed by one receiver should not exceed four.

Figure 7 illustrates the influence of noise on spectrum estimates. The basic spectra were calculated for every second data block in the sequence, and three interpolated spectra were inserted between each pair of blocks. The top panel is the same as in Figure 6. The rest of the plots show (from top to bottom) the AR dynamic spectra estimated for the signal-to-noise ratio of 40 dB, 20 dB, and 10 dB, respectively, which corresponds to almost the entire range of SNR values encountered in experiments. It can be seen that the quality degrades both with an increase in the noise level and with its decrease. The latter is the well known fact that the order of the AR model rapidly decreases in the process of fitting the model coefficients. As a consequence, the width of spectral lines increases. Nevertheless, the quality of the results appears to be quite satisfactory in all cases presented in Figure 7.

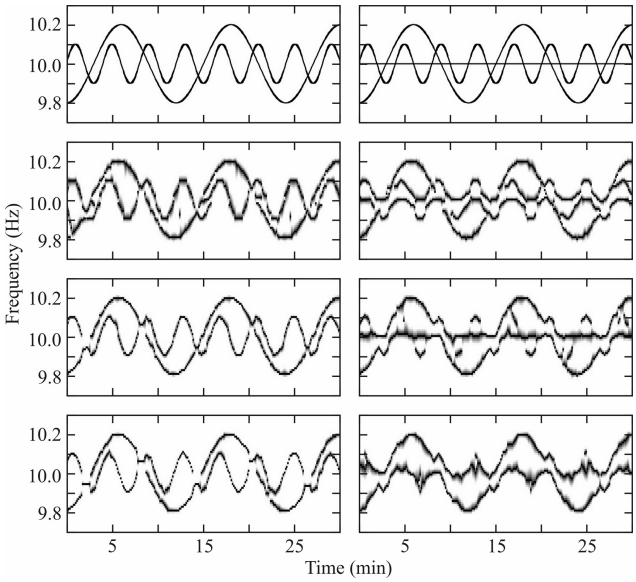

Figure 7. Model processes (top panels) and AR dynamic spectra for the 40 dB, 20 dB, and 10 dB signal-to-noise ratio (2nd, 3rd, and 4th from top to bottom panels, respectively). The intervals between 12.8 s segments of the random process are equal to 30 s.

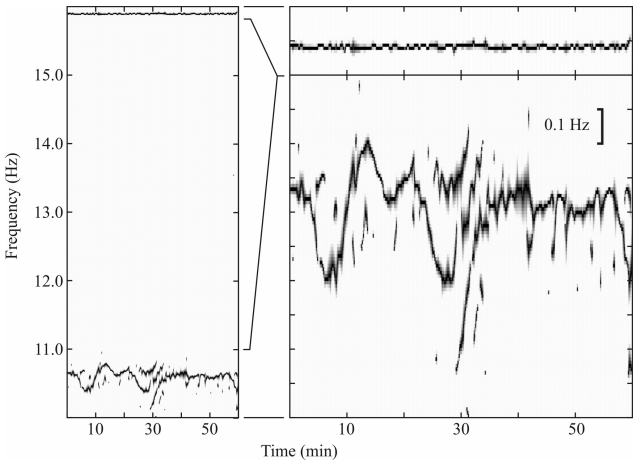

Figure 8. Dynamic spectra of the 4.2 MHz signal passing over a 50 km daylit circuit on September 22, 2010. At the top of the figure is shown the spectrum of the frequency stabilized local oscillator signal and at the bottom, the dynamic spectrum of the simultaneously recorded ionospheric signal.

Figure 8 demonstrates the time-frequency stability of the upgraded passive radar. Here, the dynamic spectra of the 4.2 MHz signal passing over a 50 km

daylit circuit are presented. The radio receiver periodically received 3.2 MHz and 4.2 MHz signals. The spectral estimation was performed by invoking the AR parameter estimation technique, when three interpolated spectra were calculated between each pair of the basic spectra. At the top left in Figure 8 are shown the spectrum of a frequency-stabilized signal simultaneously fed to the receive antenna from the C6-31 synthesizer and, at the bottom left, the spectrum of the 4.2 MHz signal reflected from the ionosphere, which is frequency up-shifted by 10.67 Hz. This frequency shift is introduced in order to determine the sign of the Doppler shift of frequency. The C6-31 synthesizer signal was not synchronized with the local oscillators of the passive radar and had a frequency of about 5 Hz larger than the frequency of the ionospheric signal. A zoomed in view of the same plots is shown on the right in Figure 8. It can be seen that the variations in the local signal frequency do not exceed ±0.01 Hz, which is approximately equal to the highest precision in frequency estimated by the computer program. This can be the case when the entire radar frequency instability is of no less than $5 \cdot 10^{-9}$. The observed Doppler shift of the ionospheric signal amounts to 0.2 – 0.6 Hz, which is considerably greater than both the highest precision in frequency estimation by the computer program and the spectral resolution of the 12.8 s data block length. Therefore, the dynamics of a spectral component can be easily monitored.

The third IF frequency mixers and low-pass filters are not used when panoramic monitoring of radio interference is performed. Instead, the ordinary amplitude demodulators are utilized, and the signal obtained passes to the ADC. The IF bandwidth is usually set equal to 6 kHz, and the sampling frequency to 10^4 samples per second. The range of scanned frequencies is chosen to be equal to either the entire receiver frequency band or its part, and the frequency step to 5 kHz. At each frequency step, a hundred of amplitude samples are measured, that are further corrected in accordance with the current settings of the attenuator, the ADC, the IFA gain, and their amplitudes and powers are averaged; the results are stored in a PC diurnal file. The maximum duration of the 1 – 31 MHz scan does not exceed 2 min. This mode of operation is auxiliary and is used to find broadcasting stations convenient for Doppler measurements, as well as to independently monitor the ionosphere.

At Kharkiv City, a Glonass receiver monitors the total electron content. Figure 9 shows variations in Glonass total electron content (TEC) during the Soyuz-U vehicle launch at 14:38:15 UT on June 21, 2011.

Radar has been designed and produced to simultaneously measure the electron density profile from the D region to the F-layer peak altitude at the Gaidary observation site. Figure 10 illustrates its capabilities.

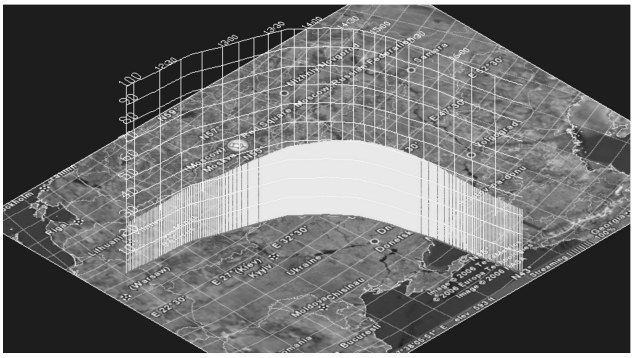

Figure 9. Universal time variations in Glonass total electron content (TEC) observed on June 21, 2011. The line on the map represents the sub-ionospheric points, the universal time is indicated at the top line, and the TEC values marked in light grey are indicated at the left-hand vertical line in TEC units (1 TEC unit = 10^{16} el m^{-2}).

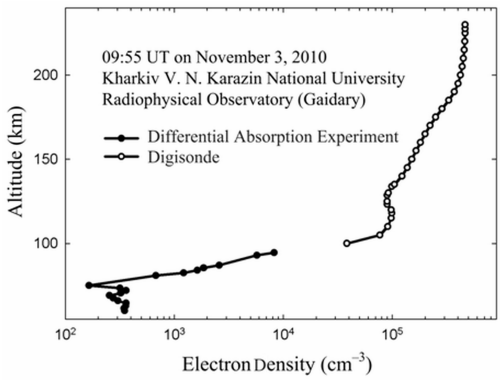

Figure 10. Electron density profiles simultaneously measured from the D region to the F-layer peak altitude.

Conclusions

Two modern automated instruments for monitoring the geospace environment in the range of geomagnetic pulsation and in hectometer and decameter radio wave bands are in operation at the Kharkiv V. N. Karazin National University Radiophysical Observatory in the vicinity of Grakovo Village (49°38'49" N; 36°56'07" E). The performance specifications of the instrumentation and the software employing modern signal processing techniques provide verified high temporal resolution measurements required for monitoring the highly variable space atmosphere interaction region. At Kharkiv City, the Glonass receiver monitors the total electron content, and the radar capable of simultaneously measuring the electron density profile from the D region to the F-layer peak altitude is installed at the Gaidary observation site (49°37'51" N; 36°19'40.1" E).

References

Garmash, K.P., Gokov, A.M., Kostrov, L.S., Rozumenko, V.T., Tyrnov, O.F., Fedorenko, Y.P., Tsymbal, A.M., Chernogor, L.F.: 1999b, Telecommunications and Radio Engineering 53 (4–5), 6.

Garmash, K.P., Leus, S.G., Pazura, S.A., Pokhilko, S.N., Chernogor, L.F.: 2003, Radio Physics and Radio Astronomy 8 (2), 163 (in Russian).

Garmash, K.P., Rozumenko, V.T., Tyrnov, O.F., Tsymbal, A.M., and Chernogor, L.F.: 1999a, Foreign Radio Electronics. Progress in Modern Radio Electronics 7, 3 (in Russian).

Marple, S. L.: 1987, Digital Spectral Analysis: With Applications, Prentice Hall, p. 492.

Rabiner, L.R., Gold, B.: 1975, Theory and Application of Digital Signal Processing, Prentice Hall, p. 762.

Tyrnov, O.F., Garmash, K.P., Gokov, A.M., Gritchin, A.I., Dorohov, V.L., Kontzevaya, L.G., Kostrov, L.S., Leus, S.G., Martynenko, S.I., Misyura, V.A., Podnos, V.A., Pokhilko, S.N., Rozumenko, V.T., Somov, V.G., Tsymbal, A.M., Chernogor, L.F., and Shemet, A.S.: 1994, Turkish J. of Phys. 18, 126